The BlackGEM telescope array

I: Overview[*]

P.J. Groot[1,2,3,4], S. Bloemen[1], P.M. Vreeswijk[1], J.C.J. van Roestel[5], P.G. Jonker[1], G. Nelemans[1,6,7], M. Klein-Wolt[1],
R. Lepoole[8], D.L.A. Pieterse[1], M. Rodenhuis[9], W. Boland[9], M. Haverkorn[1], C. Aerts[1,6,10], R. Bakker[11], H. Balster[1],
M. Bekema[9], E. Dijkstra[9], P. Dolron[1,11], E. Elswijk[9], A. van Elteren[8], A. Engels[11], M. Fokker[1], M. de Haan[9],
F. Hahn[11], R. ter Horst[9], D. Lesman[9], J. Kragt[9], J. Morren[6], H. Nillissen[1], W. Pessemier[6], A. de Rijke[12], G. Raskin[6],
L.H.A. Scheers[12], M. Schuil[9], S.T. Timmer[1], I. Arcavi[13], N. Blagorodnova[14,15,16,1], S. Biswas[1], R. Breton[17],
H. Dawson[18], P. Dayal[19], S. De Wet[2,3,4], C. Duffy[29], S. Faris[13], M. Fausnaugh[20], A. Gal-Yam[21], S. Geier[18],
A. Horesh[22], C. Johnston[1,6,23], R.A.D. Wijnands[5], D. Modiano[5], G. Katusiime[14,15,16], C. Kelley[1], A. Kosakowski[20],
T. Kupfer[20,24], G. Leloudas[25], O. Mogawana[2,3,4], J. Munday[26], J.A. Paice[27], F. Patat[28], I. Pelisoli[26], G. Ramsay[29],
P.T. Ranaivomanana[1,6], R. Ruiz-Carmona[22,30], V. Schaffenroth[18,31], S. Scaringi[27], F. Stoppa[1], H. Tranin[14,15,16],
M. Uzundag[6], S. Valenti[32], M. Veresvarska[27], H.C.I. Wichern[25], R.A.M.J. Wijers[5], and E. Zimmerman[21]

(Affiliations can be found after the references)

ABSTRACT

The main science aim of the BlackGEM array is to detect optical counterparts to gravitational wave mergers. Additionally, the array will perform a set of synoptic surveys to detect Local Universe transients and short time-scale variability in stars and binaries, as well as a six-filter all-sky survey down to ~22nd mag. The BlackGEM Phase-I array consists of three optical wide-field unit telescopes. Each unit uses an f/5.5 modified Dall-Kirkham (Harmer-Wynne) design with a triplet corrector lens, and a 65 cm primary mirror, coupled with a 110Mpix CCD detector, that provides an instantaneous field-of-view of 2.7 square degrees, sampled at 0.564″/pixel. The total field-of-view for the array is 8.2 square degrees. Each telescope is equipped with a six-slot filter wheel containing an optimised Sloan set (BG-*u*, BG-*g*, BG-*r*, BG-*i*, BG-*z*) and a wider-band 440-720 nm (BG-*q*) filter. Each unit telescope is independent from the others. Cloud-based data processing is done in real time, and includes a transient-detection routine as well as a full-source optimal-photometry module. BlackGEM has been installed at the ESO La Silla observatory as of October 2019. After a prolonged COVID-19 hiatus, science operations started on April 1, 2023 and will run for five years. Aside from its core scientific program, BlackGEM will give rise to a multitude of additional science cases in multi-colour time-domain astronomy, to the benefit of a variety of topics in astrophysics, such as infant supernovae, luminous red novae, asteroseismology of post-main-sequence objects, (ultracompact) binary stars, and the relation between gravitational wave counterparts and other classes of transients.

Key words. optical telescopes – synoptic surveys – transients – gravitational wave astronomy

1. Introduction

The direct detection of gravitational waves (GW) through the use of laser-interferometry has opened up a completely new window onto the Universe (Abbott et al. 2016). To fully utilise the scientific promise of this new domain, gravitational wave sources also need to be identified, where possible, in the electromagnetic (EM) window. The detection and subsequent follow-up of the binary neutron star merger GW 170817 has shown the wealth of (astro)physics that can be determined from a combined GW+EM detection (e.g. Abbott et al. 2017a, Abbott et al. 2017b). Well before the detection of GW 170817, it had become clear that sky localisation and sensitivity would be the key issues in a successful EM detection of a GW source, e.g. Nissanke et al. (2013). The localisation capabilities of ground-based laser-interferometers are ultimately limited by the speed of light and the size of the Earth. This results in localisation uncertainties ('error boxes') of tens to thousands of square degrees, depending on the signal-to-noise (SNR) in the GW band, the number of laser interferometers, the orientation of the source location

and spin angles with respect to the (plane of) detectors on Earth (e.g. Fairhurst 2011, Nissanke et al. 2013, Abbott et al. 2020, Petrov et al. 2022). Model analyses of expected EM signatures show that the optical-infrared regime is favourable for an EM detection due to the non-relativistic, semi-isotropic nature of the radiation emitted in a gamma ray burst (GRB) afterglow-like and kilonova-type event, on timescales of hours to days after the merger event itself (e.g. Kasen et al. 2013, Rosswog et al. 2014, Grossman et al. 2014, Setzer et al. 2023, Kawaguchi et al. 2020). Peak apparent magnitudes of kilonova events are expected to be in the range 17–23 mag for binary neutron star mergers up to a GW detection horizon of d_{hor} ~<200 Mpc for the current generation of laser interferometers for a binary neutron star merger, depending on a multitude of, so far poorly constrained, parameters such as the total ejected mass, the exact composition of the material and the observer's viewing angle to the event. Efforts to establish the counterparts to a set of GW events and limit the brightness of kilonova counterparts include Kasliwal et al. (2020), Andreoni et al. (2020), Gompertz et al. (2020), and de Wet et al. (2021).

---

[*] www.blackgem.org

1.1. Science requirements

The BlackGEM array aims to detect optical kilonova signatures of gravitational wave mergers in the kilohertz regime on a timescale of minutes to hours after the merger event. Coupling the expected error box sizes and brightness expectations, the following science requirements were formulated at the start of the project (2012):

*SR*1: The ability to detect an optical counterpart to a GW merger, down to a brightness of 23rd magnitude in New Moon conditions in a broad band filter;

*SR*2: within an error box of up to 100 square degrees;

*SR*3: on a timescale of no more than 2 hours;

*SR*4: with a start of observations no later than 10 minutes after the GW alert.

1.2. Design requirements

The science requirements led to the following design requirements:

*DR*1: A spatial resolution limited by the natural seeing on a high-quality site, nominally taken to be $1''$, to take advantage of the trade-off between depth, aperture and spatial resolution in background-limited observations;

*DR*2: A set of filters spanning the full optical window, including a broad-band filter optimised for throughput;

*DR*3: A data-reduction pipeline capable of processing and analysing the acquired data on time scales initially set to 10 minutes to allow for rapid identification of counterpart candidates;

*DR*4: A robotic set-up for autonomous follow-up of a GW event.

Requirement *DR1* follows from the required depth of observations. In the sky-background limited regime, the achieved signal-to-noise ratio for point sources scales as the square of the telescope diameter (D) over the achieved image quality ("seeing", σ), i.e. $SNR \propto (D/\sigma)^2$, and therefore excellent natural seeing can be used to trade-off against mirror diameter to limit the size (and cost) of a facility. The most restrictive of the science requirements is the combination of wide-field and image quality/depth. An assessment of available facilities and off-the-shelf telescopes showed that no viable option was available in the southern hemisphere that could simultaneously accomplish all science requirements. This gap in facility coverage in the Southern Hemisphere and the long-term membership of the Netherlands in the European Southern Observatory (ESO) determined the choice for a Chilean site, in particular ESO La Silla. Since the start of the project, other Southern Hemisphere coverage gaps have been filled in by the BlackGEM prototype MeerLICHT and ATLAS-Sutherland in South Africa (and the ATLAS station in Chile), as well as the GOTO-South telescopes in Australia, effectively now giving 24/7 coverage of the southern skies (Bloemen et al. 2016, Tonry et al. 2018, Steeghs et al. 2022).

Design requirement *DR2* comes from the unknown/uncertain colour of kilonovae, and the expected strong reddening of kilonovae in the first few hours-day, as simulated by e.g. Kasen et al. (2013) and demonstrated by GW 170817 (e.g. Arcavi et al. 2017). Having a set of filters available will allow BlackGEM to both choose the best filter for an observation as well as determine optical colours for transients found in the error box, where fast reddening is expected to be a strong diagnostic to distinguish

kilonovae from, for example, young supernovae and/or Galactic transients, in particular, dwarf novae outbursts (see e.g. van Roestel et al. 2019a, de Wet et al. 2021).

Design requirement *DR3* follows directly from *SR3* and *DR4* from *SR4*. To achieve *SR2*, an instantaneous field-of-view of ≥8 square degrees was needed, and this has been achieved by building a 3-unit array. The BlackGEM unit telescopes are labeled BG-2 ("Ruby"), BG-3 ("Opal"), and BG-4 ("Emerald"; see Sect. 2.7)[1].

2. Optomechanical Design

The project has opted for an array of smaller unit telescopes with single-detector cameras over a monolithic telescope and/or mosaic detector approach. This was motivated by costs, as a unit telescope could be kept smaller, with less-demanding (slower) and smaller-sized optics, and the added possible benefit of series production, and the difficulty in mosaic cameras to properly align individual chips with each other, as well as to a, generally curved, focal plane, see e.g. the additional measures taken by the Zwicky Transient Facility (ZTF, Bellm et al. 2019). The choice was made for an equatorial mount over an alt-az mount to avoid the added complication of a derotator for the camera, as well as the fact that, in alt-az telescopes, the diffraction spikes of bright stars rotate with respect to the sky depending on the parallactic angle, potentially leading to a large number of spurious transients and/or variables (Toma et al. 2016). Smaller optics allow the use of a filter wheel, housing filters of reasonable size (~10 cm). After the optical design was made, it was realised that even an Atmospheric Dispersion Corrector (ADC) could be accommodated (ter Horst et al. 2016).

2.1. Optical design and manufacturing

The optical design of the BlackGEM unit telescope is that of a modified Dall-Kirkham (Harmer-Wynne; Harmer & Wynne 1976) design consisting of a parabolic primary mirror, a spherical convex secondary mirror and a triplet lens field-corrector. After the triplet lens, which doubles as the ADC, light passes through a filter and the entrance window to the cryostat to fall onto the detector. The parameters of the optical elements are given in Table 1. The focal ratio of the combined system is F/5.5, resulting in a focal length of $F_z = 3300$ mm, with the z-axis taken along the optical path. This results in a plate scale at the focal plane of 16 μm/arcsecond. Eighty per cent of the enclosed energy lies within a 9 micron radius even at 1.1° away from the optical axis, and the optical design is close to diffraction-limited at all angles away from the optical axis. The focal plane is flat to within 5 μm over a radius of 150 mm from the optical axis. At the focal plane, the lateral displacement with wavelength is less than 5 μm.

Chromatic focus variations are within $\Delta z < 10$ μm over the full focal-plane, and vignetting is limited to < 10% at the outer radius of the focal plane. The contribution of the optics to the point spread function is < 0.3″ over the full focal plane.

The fused-silica parabolic primary mirror (M1) is 65 cm in diameter, oversized with respect to the 60 mm optical aperture, to correct for the fact that the pupil is located on the secondary mirror, M2. The primary mirror was shaped by Lockwood (Illinois, USA). The primary mirrors show a peak-to-valley (PV) rms

---

[1] Numbering starts at '2' as the BlackGEM prototype MeerLICHT, installed at SAAO Sutherland, South Africa, is number 1

Table 1. Optical design of the BlackGEM telescopes. Mirrors are referred to as 'M', lenses with 'L', and surfaces on lenses with 'S', followed by a numerical label indicating their order with respect to the (incoming) light path.

	Radius (mm)	Thickness/*distance*[a] (mm)	Material	Diameter (mm)
M1	−3411.50	*−1010.90*	Fused Silica	650
M2	−2956.00	*634.00*	Fused Silica	260
L1,S1	−2201.48	25.00	BK7	200
L1,S2	−678.55	*52.47*	-	-
L2,S1	1999.58	20.00	BK7	190
L2,S2	302.68	*17.67*	-	-
L3,S1	466.73	20.00	BK7	180
L3,S2 (ADC)	1669.17	*532.38*	-	-
Filter, S1	infinity	3	Fused Silica	119x119
Filter, S2	infinity	*10*	-	-
Cryo-window, S1	infinity	12	Fused Silica	160x160
Cryo-window, S2	infinity	*10*	-	-
Detector	infinity	-	-	100x100

[a] distances from the reference plane are given in italics

of $\lambda/5$ (BG-2), $\lambda/2$ (BG-3), and $\lambda/3$ (BG-4) at a reference wavelength of $\lambda = 650$ nm. The lower accuracy value of BG3 is due to residual astigmatism that proved to be present in the primary mirror shape after production. This has been partially corrected by a tensioning clamp.

The fused-silica spherical secondary mirror was made at Schott, Switzerland, and then polished in-house at the Netherlands Research School for Astronomy (NOVA[2]) Optical-Infrared group. Performance tests show a root-mean-square variation of 58 nm, $\lambda/9$ wavefront error, at the reference wavelength of $\lambda = 500$ nm.

The triplet lens field corrector was manufactured at FineOptix, Germany. Anti-reflection coatings are put on all transmission optics to suppress ghosting, required by the combination of the desire to detect faint (23rd mag) transients and a wide field-of-view which will always contain stars of $<10^{th}$ magnitude that can cause a significant reflected-light background.

To obtain maximum throughput over the full wavelength range (0.3 - 1.0 μm), both the primary and secondary mirrors were initially coated with UV-enhanced protected silver coatings with very high reflectivity ($> 90\%$) at $\lambda > 350$ nm. However, during commissioning, this coating very quickly tarnished on all mirrors. In collaboration with NOIRLab[3] and ESO, the original protected silver coatings on both M1 and M2 were replaced with a protected silver coating on M1 and a bare aluminium coating on M2.

The BlackGEM telescope uses an ADC as part of the field-flattening optics (ter Horst et al. 2016). The third lens in the triplet lens field-corrector can be moved in the plane perpendicular to the light path by two rotating notch actuators. Due to its plano-concave shape, this lens thereby acts as a prism when it is off-centred, which, at the right position, gives a full-field first-order atmospheric dispersion correction. This allows the BlackGEM telescopes to remain seeing-limited in blue and broad-band filter observations up to zenith distances of 60°.

2.2. Filters

The BlackGEM filter set is similar to the Sloan set (u, g, r, i, z, Doi et al. 2010) with the addition of a wider-band, 440-720 nm,

Table 2. Passband of the BlackGEM filters. Start and end wavelengths are defined as the wavelengths where 1% transmission is crossed.

Filter	Start Wavelength (nm)	End Wavelength (nm)
u_{BG}	346	410
g_{BG}	409	551
q_{BG}	437	722
r_{BG}	559	690
i_{BG}	687	843
z_{BG}	837	994

q-band filter. The filter response curves were optimized for the overall throughput and steepness of the flanks. The change-over from 1%–99% transmission occurs within 10 Å for all filters on both sides of their wavelength ranges. This sharp change-over was chosen to minimise the effect of back-reflection of light off of the filters, thereby suppressing the halos of saturated stars as well as the contribution to the background by scattered light. With the BlackGEM field-of-view, it is unavoidable to have bright stars ($g < 10$) in the field, whose scattered light can significantly contribute to the background level if the optics are not properly designed and manufactured. The g_{BG} and r_{BG} filters were purposefully separated by 8 nm, such that the strong sky emission line of [OI] 557.7 nm falls in neither of the two filters.

The BlackGEM filter set was designed and made at Astrodon Inc (USA), now part of Optical Structures Inc. An overview of the measured transmission curves is given in Table 2, Fig. 3 and the 5 Å-step throughput values are given in App. A.

The filters are housed in a six-slot filter wheel, which can be rotated in both directions and is located in the camera house, which is between the lens barrel and the entrance window to the cryostat. Filter changes take up to ~3 seconds between the extreme positions.

2.3. Detector & Cryostat

Each BlackGEM unit telescope uses a single STA1600, 10 560 ×10 560 pixel, CCD detector with a square pixel size of 9 μm × 9 μm. The detectors were produced at Semiconductor Technology Associates (USA) and are equipped with a broadband
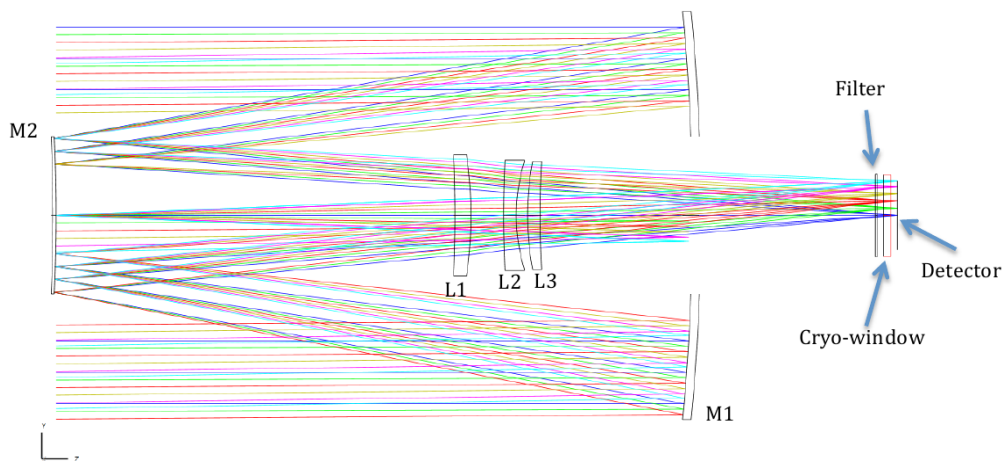
Fig. 1. Optical layout of the BlackGEM telescopes. Coloured lines show principal and off-axis ray paths. Mirrors ('M') and lenses ('L') are indicated.
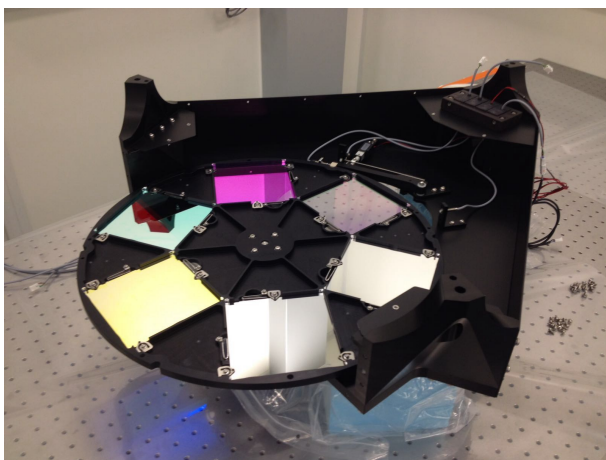

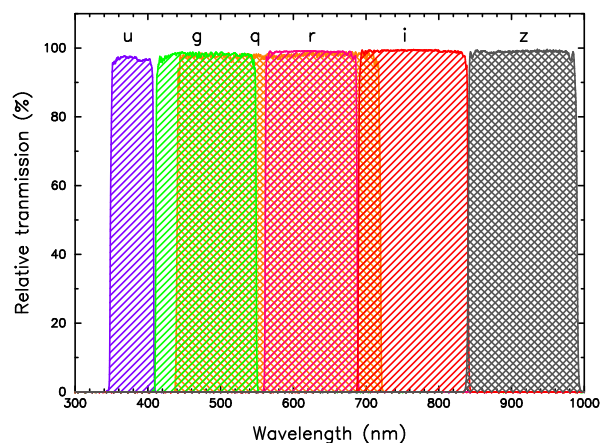**Fig. 2.** Photo of the opened filter wheel during assembly.

Fig. 3. Transmission curves of the BlackGEM filters. Blue is the *u*-band, green the *g*-band, black the *q*-band, red the *r*-band, orange the *i*-band and in pink the *z*-band.

coating. The quantum efficiency curve is shown in Fig. 4. All BlackGEM detectors have a very low number of bad pixels and columns, $\ll 1\%$, and a few minor blemishes with lower quantum efficiency (QE).

Each detector is read out through an STA Archon controller via 16 ports over four video boards at 1 MHz read-out speed. The set-up results in a 7s read-out time and a read-out-noise of 7–8 electrons. Some cross-talk is present over the channels, which is corrected for in the data reduction process.

The detector's cryostat was designed and manufactured at the Institute for Astronomy at the KU Leuven (Raskin et al. 2016). The cryostat design was inspired by that of the cryostats of the MAIA instrument at the Mercator telescope on La Palma (Raskin et al. 2013). The detector is cooled by a Joule-Thomson cooler (Polycold Compact Cooler) using PT16 gas. A heater inside the cryostat stabilizes the detector temperature at 160 K to within 0.1 K. The cryostat is controlled by a PLC controller, custom-built at the KU Leuven (Raskin et al. 2016). An overview of the cryostat design is given in Fig. 5.

Combined with the optical design of the telescope, the resulting field-of-view of each BlackGEM unit telescope is 1.65° × 1.65° sampled at 0.564″/pixel. The three-unit array currently installed at La Silla gives an 8.2 square degrees instantaneous field-of-view. The system throughput curves, including the at-mosphere, the mirrors, the lenses, the filters and CCD window and the detector are shown in Fig. 6 and listed in Tab. A.2.

2.4. Mechanical design

The mechanical design of the optical telescope assembly (OTA) was made at the NOVA Optical Infrared Group and needed to comply with the requirement that optical performance remains seeing limited (i.e. optical distortions $\leq 0.3''$) at 60° zenith distance over an integration time of 60 seconds. Also, the complete structure needs to be able to withstand wind loads up to 15 m s^{-1} in an open clam-shell dome. This resulted in stringent requirements on the stiffness of the OTA, requiring an all carbon-fiber design (Figs. 7 and 8). This was designed with, and manufactured by, Airborne BV (The Netherlands). The OTA consists of a main ring, which attaches to the mount through an interface plate; trusses that connect to the top ring; and the top ring, which holds the M2 unit, connected to the OTA by a spider consisting of four blade-springs. The main ring is open at the back, leaving M1 exposed to the air in order to improve the thermal balance
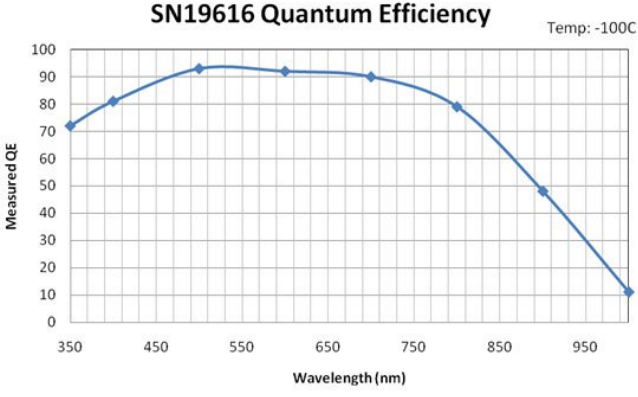
Fig. 4. Quantum efficiency as a function of wavelength for the STA 1600 detector used by the BlackGEM array. Diamonds indicate measured wavelengths.

Fig. 6. Overall relative transmission of the BlackGEM telescope system, from the top of the atmosphere to the detector, as a function of wavelength

The triplet corrector lens in its barrel is mounted to the whiffle tree assembly which also supports M1. The barrel is positioned through the central hole of the primary. The primary mirror maintains its lateral position by the lens barrel location.

The camera house with the six-slot filter wheel also contains the shutter, which is a butterfly-type shutter. Two apertures are cut such that they provide uniform illumination per pixel over the focal plane during the length of an exposure (Fig. 9). The shutter takes ~0.8 second to cross the focal plane. This limits the accuracy of the BlackGEM timing. More accurate timing requires a 'per-pixel' illumination model. Timing for BlackGEM observations is provided by a trigger from the shutter controller to a GPS-based Meinberg LANTIME M3000 clock. Both 'shutter open' as well as 'shutter closed' GPS times are recorded, and the mid-time of each observation is derived from these two triggers.

2.5. Focus and guiding

After an initial positioning and alignment of the main optical elements, focus is controlled through a PI P-528.TCD piezo-stage on which M2 is mounted. The stage can be moved over a $200\,\mu m$ range along the optical axis. Collimation is done manually by shifting and tilting M1.

The lateral movement of the piezo stage allows for a $\pm 200''$ offset from the nominal position of the optical axis. This range is used for autoguiding through three guide cameras mounted at the sides of the main field-of-view next to the science CCD. The guide cameras are UI-3060CP-M-GL Rev.2 from IDS Imaging and are operated through a USB-3.0 connection to the M2 control computer located in the counterweight.

The guide cameras contain a 1936×1216 pixel CMOS detector. With a plate scale of 5.86 μm/pixel (0.36″/pixel), the field of view of each camera is 11.8′×7.4′. In standard operations, a position offset is calculated from the set of guide stars detected on the three cameras at a rate of 1 Hz. Guiding is started on the 'shutter open' signal generated by the CCD controller and stopped by the 'shutter close' signal. As the guide camera pick-off mirrors are located before the shutter/filter wheel, guiding is done in white light and is independent of the chosen filter.
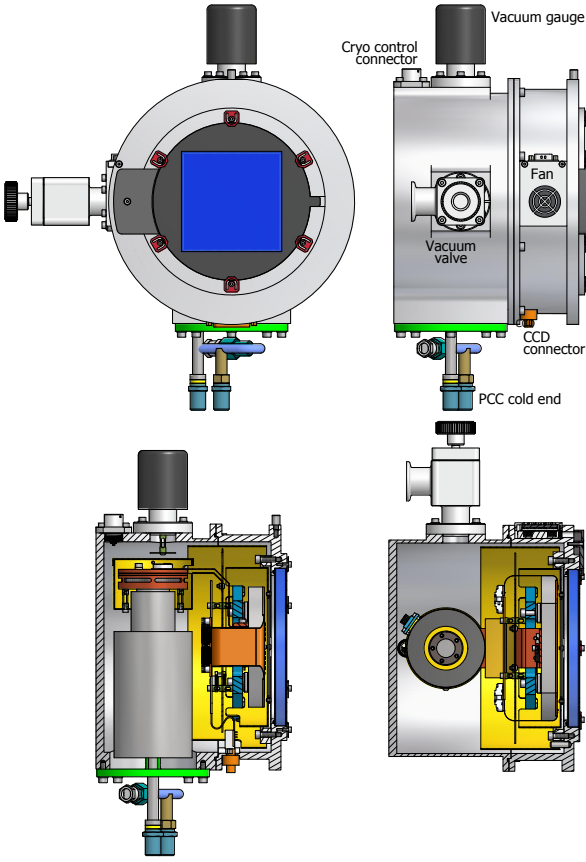

Fig. 5. Cross-cut through the design of the BlackGEM cryostat for the STA 1600 CCD detector.

between the optics and the environment. M1 is supported by an 18-pad whiffle tree, allowing precise positioning and position-independent support of the mirror. Thereby, the shape of the mirror (which is not actively controlled) remains within specifications up to 70° zenith distance. Connected to the main ring by blade connectors is the camera unit, holding the filter and shutter wheel in a closed compartment and the cryostat/detector assembly. The M2 unit holds the secondary mirror which is itself mounted on a piezo stage that allows for tip-tilt control, used for guiding, and lateral motion along the optical axis, used for focussing.
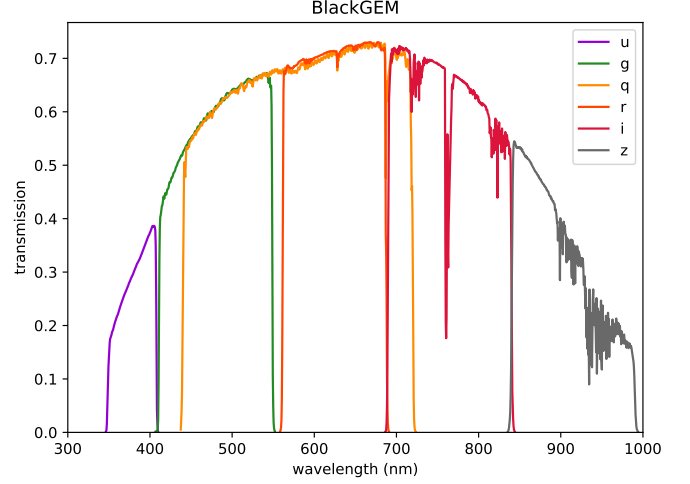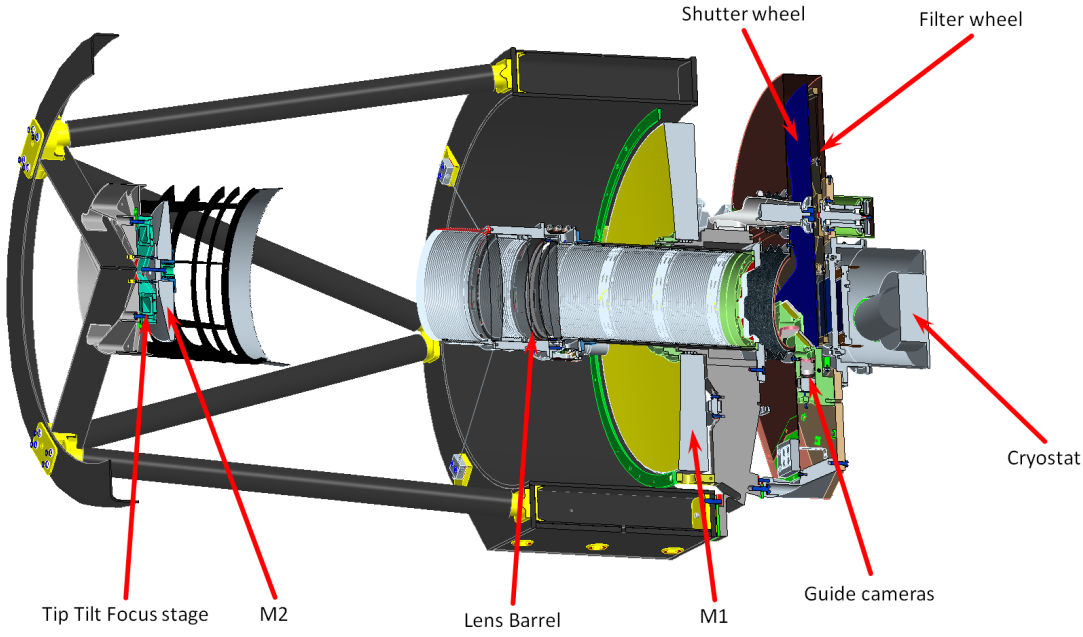
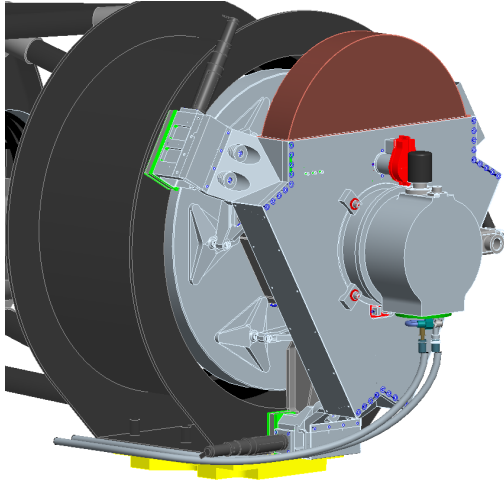**Fig. 7.** Annotated design drawing of the BlackGEM telescopes.

Fig. 8. Backside view of the mechanical design of the BlackGEM telescope. At the far left, the carbon-fibre mirror cell (black) can be seen with the main mirror (grey) supported on an 18-point, 6-pad, 3-arm whiffle tree. The shutter/filterwheel housing and the cryostat (brown/grey) are attached to the carbon fibre mirror cell on three spring-blade clamping points (green). The attachment to the mount is via an interface plate, which is part of the carbon-fibre mirror cell (yellow).
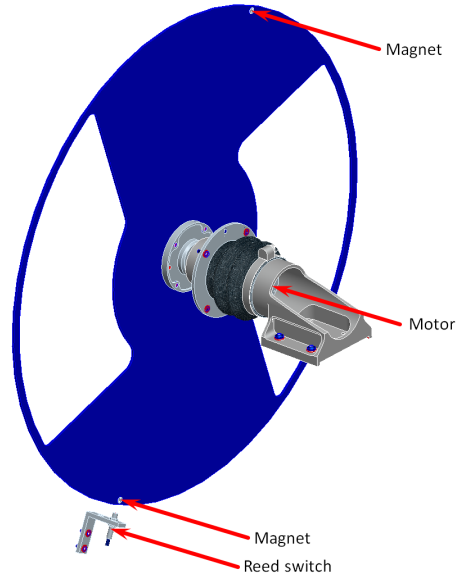

Fig. 9. Butterfly design of the BlackGEM shutter, showing the curved sides that ensure equal illumination per pixel during opening and closing of the shutter.

2.6. Mount and Cable wraps

Each BlackGEM telescope is mounted on its own second generation Fornax-200 mount, a German equatorial mount which was co-designed by the BlackGEM project and the Fornax company (Hungary). The mount consists of two identical drive systems, one for declination and one for hour angle. Each drive consists of a worm wheel of 605 mm in diameter with 250 cogs, in a worm - worm wheel ratio of 1:250. The wheels are made of bronze for stiffness and durability. A set of Renishaw absolute encoders are used for pointing and allow a precision ≤ 0.1″. In practice the pointing accuracy is limited by physical effects such as flex-ure of the structure, play between gears etc, to about 1′, which is acceptable given the large field-of-view. A second generation mount controller fully using the absolute encoders is under development.

Some of the telescope's electronic subsystems (filter-wheel/shutter controller, piezo controller, ADC controller, M2 control computer, DC power supplies) are located in the counterweight to serve as part of the counterweight. Only the CCD controller is placed as close as possible to the cryostat to prevent electronic pick-up noise. The counterweight, the CCD controller, and the guide cameras are water/glycol-cooled to prevent heat-dumping near the telescope.

Cabling from the telescope down to the computer rack goes via a cable wrap on the declination axis first and then through a second wrap behind the hour angle axis. The cable wraps are made of a caterpillar type commonly used in astronomical telescopes where a flexible tray allows freedom of rotation in excess of one full rotation (see Fig. 10).
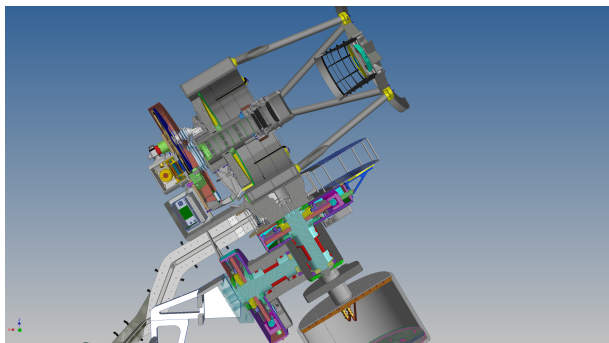

Fig. 10. Cut-open view of the BlackGEM telescope on the Fornax 200 mount, also showing the drum-shaped counter-weight and the fly-over cable wrap

2.7. Dome, housing and site

Each telescope is mounted on a triangulated pyramidal pier consisting of hollow steel pipes to maximize stiffness (Fig. 11). The pyramidal pier itself is bolted onto on a steel 1m diameter hollow cylinder, 5m in height. The telescope pier is nested inside a second steel pier, 1.3m in diameter, which holds the observing floor and an Astroshell 5m diameter clam-shell dome. The telescope and dome pier are separately anchored in concrete feet and only connect to each other through the La Silla bedrock. The rotation centre of the mount is located 8m above the ground and 3m above the floor of the dome. Due to the position of the telescope on the west side of the pier, observations towards the east are taken with the telescope high up, above the mount, whereas observations towards the west have the telescope lower to the dome floor. This also limits the visibility to the West to +3hr in hour angle.

At La Silla, the BlackGEM array is located on the site of the former GPO/Marly and Marseille telescopes, at the top of the 'ridge'. The former Marseille building now functions as the BlackGEM control room and warehouse building, also housing the cryocoolers, control servers, power and networking systems. Internet- and power-wise the BlackGEM array is completely integrated into the ESO La Silla infrastructure and is one of the hosted projects. An overview photo is shown in Fig. 12. The layout of the site has been made such that a maximum of 15 Black-GEM telescopes can be accommodated on the former GPO 'island'.

The geographic location of each of the three BlackGEM telescopes is given in Table 3. All telescopes are at the same altitude of 2382 m with respect to the Earth's ellipsoid (McCarthy & Petit 2004), and aligned along an East-West line, with BG2 being the eastern-most telescope and BG4 the western-most telescope.

3. Telescope Control system

BlackGEM is controlled through the ABOT system developed by Sybilla Technologies (Poland). The ABOT system is derived from the Solaris project (Kozłowski et al. 2017). A web-interface
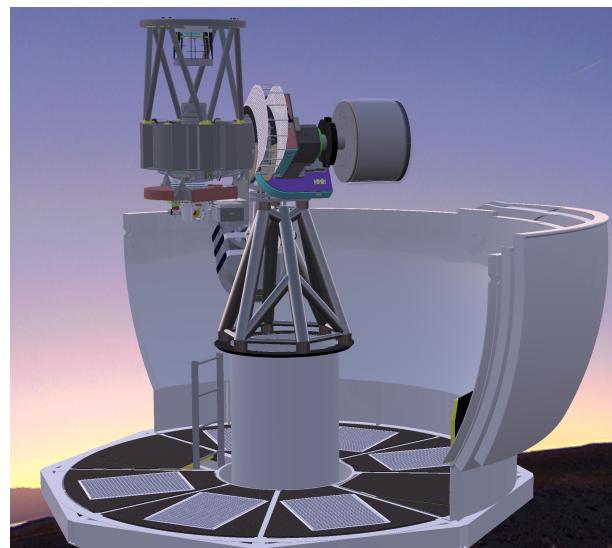

Fig. 11. Design overview of a BlackGEM unit telescope and counter-weight attached to the Fornax mount (purple/green) and the pyramidal pier and steel cylinder base. A cut-open version of the clam shell dome in the open state is shown.

Table 3. Geographic location of the BlackGEM telescopes

Telescope	Longitude (d)	Latitude (d)
BG-2 (Ruby)	−70.737850	−29.257469
BG-3 (Opal)	−70.737969	−29.257469
BG-4 (Emerald)	−70.738067	−29.257469

and cloud-based observing queues are used to control the telescope remotely and/or robotically. Dedicated procedures have been defined with Sybilla to robotise the taking of flatfields, biases, and regular science data.

The PLC-based ObservatoryWatch system supplied by Cilium Technologies (Poland) monitors weather sensors and supplies this information to the ABOT system. It also supplies a direct trigger to the dome in case of adverse conditions, which ensures that the dome is closed even if ABOT is not operational. The ABOT telescope control system interfaces with the Microsoft Azure cloud platform, which allows access to the system from anywhere in the world.

4. Data processing

All raw data are transported in real-time from La Silla to Santiago de Chile, where they are ingested into the Google Cloud environment. Final data products (calibrated images, source catalogues, and transient catalogues) are available within (currently) 15 minutes after the end of the exposure. A full description of the BlackGEM data processing and data products will be described in Vreeswijk et al. (in prep.), hence only a short summary is given here.

All BlackGEM data are debiased and (twilight-sky) flatfielded. No defringing is required for the redder bands due to the very low levels of fringing in the STA 1600 detector. Astrometric calibrations are made using positions from the Gaia Data Release (DR) 3 astrometric catalogue, and all BlackGEM positions are in the ICRS frame with epoch J2016.0 (Lindegren et al. 2021; Gaia

Fig. 12. Aerial view of the BlackGEM array site at ESO La Silla, seen from the south-east. The BlackGEM control building, formerly belonging to the Marseille telescope, can be seen in front of BG-2 and BG-3. The ExTra, ESO 1m, REM and ESO 1.5m telescopes can be seen to the North of BlackGEM.

Collaboration et al. 2023). Astrometric solutions generally show root-mean-square residuals <50 μas in each coordinate.

Photometric calibrations are performed using the Gaia DR3 low-resolution spectra of selected stars in the field-of-view. A set of 70 million Gaia DR3 low-resolution spectra were convolved with the BlackGEM throughput curves, taking the La Silla atmospheric extinction into account. Synthetic BlackGEM-system apparent magnitudes were generated for all stars in the reference catalogue. For selected stars in each frame the zeropoint is deduced by comparing the measured instrumental magnitudes with the reference magnitude. From the resulting histogram of zero-points a median value, as well as a zeropoint accuracy, is derived. A quality control step is performed where, based on a number of performance statistics, including e.g. the zeropoint, the limiting magnitude, the derived image quality, the elongation of stars etc., the frame is classified in one of four ranges, running from 'green', to 'yellow', 'orange' and 'red'. Everything but red-classified frames can be used for science.

Using a reference frame, image differencing is performed using the ZOGY formalism (Zackay et al. 2016). From the resulting corrected statistics (SCORR) map, transients and variables are identified when their SCORR value is larger than 6, corresponding to a > 6σ deviation from the mean noise pattern in the difference image. All objects thus identified are saved in a 'transient catalogue'. These include positive as well as negative transients and variable objects. A real-bogus machine-learnt algorithm is then applied to each detection to produce a real-bogus score between 0 (bogus) and 1 (real) (Hosenie et al. 2021).

In addition, a match is made to all possible asteroids within 20″, as known to the Minor Planet Center (MPC) (Pieterse et al., in prep.). The current MPC database is downloaded on a daily basis at 17:00 local time.

On each reduced frame, a forced optimal-photometry measurement (Horne 1986) is made at the position of all Gaia DR3 objects within the field of view, where proper motion has been taken into account. The output from the forced optimal-photometry routine is saved in the 'full-source catalogue'. The transient database is incorporated into a query-able MonetDB

database provided by DataSpex BV in the Netherlands. The full-source database is a Google BigQuery database, implemented into the GoogleCloud environment by the Dutch branch of Cloud Technology Solutions.

5. Operations

The BlackGEM telescopes are robotically operating at the ESO La Silla Observatory. The daily routine consists of:

– Biases: a set of five biases taken each afternoon before sunset and each morning before sunrise in a closed-up dome;
– Flatfields are taken each twilight for each of the six filters, with 5 exposures per filter using dynamic exposure times to obtain, on average, 13 000 counts per pixel in each flatfield. The filters are ordered as u,z,r,g,i,q during the evening twilight and the reverse for the morning twilight. This order is set by the combined effects of system throughput in a given filter and the darkening (brightening) evening (morning) sky. Flatfields are taken at a telescope position of Dec =−29°, HA = 1hr away from the direction to the Sun. A 10″ dither in both RA and Dec is applied between each flatfield exposure in a filter sequence;
– Survey program: 50 minutes after sunset, the night program starts. During the day, a survey plan will have been generated with a priority (from 1, lowest to 5, highest). During normal operation, this survey plan will be executed, unless it is overridden by an automatic trigger, in particular for the GW program.

Each BlackGEM telescope is mounted on the west side of the pier, to allow for a maximum eastern hour angle in detecting GW afterglows events at the earliest possible time. No meridian flip can be performed due to the fixed cable wraps. Operating limits for the BlackGEM telescopes are:

– a pointing limit of > 20° above the horizon in elevation;
– a pointing limit of $HA > −7$ hrs on the east side of the pier (as long as it does not conflict with the horizon limit);

- a pointing limit of $HA < +3$ hrs on the west side of the pier due to vignetting by the bottom ring of the dome;
- a hardware limit of $Dec < +30°$, due to a hardware stop on the declination axis.

6. Science Program

The BlackGEM array is designed and built for the identification and characterisation of gravitational wave counterparts. To enable this search, and in-between GW triggers, a fixed set of survey programs will be executed. Full details on the survey program of BlackGEM will be given in an accompanying paper (Van Roestel et al., in prep) and are therefore omitted here. We provide a concise description here, to highlight the broad potential of science cases to be covered with BlackGEM.

6.1. Sky grid

All BlackGEM observations are executed on a predefined sky grid. If specific targets are requested they will be executed on a 'snap-to-grid' basis. The existence of the predefined grid strongly simplifies data reduction procedures, e.g. with respect to reference frames, as well as database structures.

The predefined grid consists of 15 946 grid points that tile the sky from the celestial South Pole up to Dec = +62°. In addition to this regular grid, 140 'special fields' have been defined that cover the baryonic mass overdensities in the nearby Universe, as well as special regions of interest in our own Milky Way Galaxy, e.g. the Galactic Bulge region, selected globular and open clusters. The special fields are labeled 16 000–16 139. The grid definition is available from the BlackGEM website[4].

6.2. Gravitational wave follow-up

The top priority of the BlackGEM science program is the follow-up of gravitational wave (GW) triggers generated by the second generation laser-interferometer detectors Advanced LIGO, Advanced Virgo, KAGRA and, in the future, LIGO-India. Simulations, e.g. (Nissanke et al. 2013) and real-world performances of LIGO-Virgo (Abbott et al. 2023) show that the expected size of error boxes in the coming phases of these GW detectors should result in sky areas of ~100–200 square degrees and detection horizon limits of ~150–200 Mpc for binary neutron star mergers and neutron star - black hole mergers when three detectors are operational. Assuming an optical brightness similar to that of GW 170817, the BlackGEM array can detect counterparts up to ~200 Mpc (Chase et al. 2022). Kilonova signals are expected to display a rapid reddening (Kasen et al. 2013), setting them apart from other types of rapid transients, with blue components (possibly) visible at early times (~hrs). For this reason, the Black-GEM telescopes have been equipped with a broad set of filters, and, if possible, a multi-colour strategy will be used.

The main requirement in the GW follow-up with BlackGEM is a cadence over the full part of the (observable) error box within 2 hrs. Scanning will be done in as many filters as can be fit into the 2-hour cadence on the observable error box. If possible, all six filters will be used. Alternatively, the u, q and i filters will be used, and in the worst case (largest error boxes), only the q-band will be used. An example of the strategy used by BlackGEM is given in de Wet et al. (2021) for the follow-up of GW 190814 with MeerLICHT and de Wet et al. (2023) for GRB 220627A. For scanning the error box, a sky grid (Sect.

6.1) will be used in conjunction with the ranked-tiling method defined in Ghosh et al. (2016). The LVK-provided localisation map is convolved with the sky grid to provide a probability per grid tile, after which the visible tiles are ordered on descending probability. Observations are made per set of ten tiles, which are then immediately repeated to veto against asteroids. Processing of data is done as outlined in Sect. 4, and candidate counterparts are sent to the BlackGEM GW team for a last-step human vetting and further processing. All validated candidates are reported to the General Coordinates Network (GCN[5]) and the Transient Name Server (TNS[6]).

As part of the GW program we will also survey a 'GW footprint' area consisting of ~2700 square degrees once a week in one filter to be able to identify recent interlopers to GW candidates, such as supernovae, tidal disruption events, dwarf nova outburts (van Roestel et al. 2019b). The sky area is targeting the majority of stellar mass within 150 Mpc.

6.3. Southern All Sky Survey

Transients can only be detected when a high-quality, deep reference frame is available. In addition, the southern skies have so far seen a limited number of (full-sky) multi-colour surveys, in particular, DELVE DR2 (Drlica-Wagner et al. 2022), VPHAS+ (Drew et al. 2014, 2016), SkyMapper (Onken et al. 2024) and the southern part of Pan-STARRS (Chambers et al. 2016). This limits the ability to construct a pre-operations reference frame from archival observations. In agreement with ESO, the Black-GEM project will therefore perform a six-band, 30 000 square degree ($\delta < +30°$) survey of the southern sky down to a depth of 22nd mag. This BlackGEM Southern All-Sky Survey (BG-SASS) will become available through the ESO Archive. As a starting point for transient detections, the BlackGEM array will use reference images obtained with the MeerLICHT prototype telescope (Bloemen et al. 2016).

6.4. Local Transient Survey

The aimed-for detection horizon to binary neutron star systems of the second generation GW detectors is, at full sensitivity, >200 Mpc. To rule out existing nearby transients as GW sources and obtain high quality data on the nearest (and brightest) transients, it is imperative to obtain a thorough and extensive set of observations of the major mass concentrations in the nearby Universe, such as the Fornax, Norma, Puppis and Eridanus galaxy clusters. In addition, within our very local Universe (<15 Mpc), a sizeable portion of nearby galaxies have been observed by the Hubble Space Telescope (HST), and contain valuable information for the identification of the progenitor stars (and their associated precursor emission) for supernova explosions (Smartt 2015; Qin et al. 2023), luminous red novae (Blagorodnova et al. 2017, 2021) and luminous blue variables (Smith et al. 2011) among others.

The Local Transient Survey of BlackGEM will include fields with major mass concentrations as well as <15 Mpc galaxies with deep HST coverage (> 300s). The observations will be done in three bands (u, q, i) with a cadence of 3 hrs. These fields will enter the watch list depending on the available slots and the visibility of each field. These fields will be kept on the list until they become unobservable due to seasonal shifts.

---

[4] www.blackgem.org

[5] gcn.nasa.gov

[6] wis-tns.org

6.5. Fast Synoptic Survey

In the last decade, the optical time-domain Universe at cadences below one hour has become available at precisions of μmag. The past *Kepler* space telescope and its refurbished K2 version, as well as the ongoing Transiting Exoplanet Space Survey (TESS) are instrumental in opening up this window of high-precision uninterrupted space photometry. This has given rise to a flood of novel science cases and discoveries aside from their prime aim of exoplanet hunting, notably asteroseismology (Aerts 2021). Periodic variables with shorter time scales of the order of a few minutes were monitored as well, with the *Kepler*/K2 and TESS short-cadence modes of about 1 minute and 20 s respectively. This delivered vastly new modelling potential for asteroseismology of compact pulsators such as white dwarfs (e.g., Hermes et al. 2017; Giammichele et al. 2018; Córsico et al. 2019) and subdwarfs (e.g. Uzundag et al. 2021). As any instrument on the ground, BlackGEM cannot deliver μmag precision nor uninterrupted light curves. However, it will be able to aid in asteroseismology of faint compact pulsators at mmag level by delivering good candidate pulsators for follow-up, from their dominant frequency accessible by BlackGEM combined with their positions in the colour-magnitude diagram, as already demonstrated from MeerLICHT photometry (Ranaivomanana et al. 2023).

Kepler/K2 and TESS also led to breakthrough science of fast accretion phenomena in various compact binaries including black holes (Scaringi et al. 2015) and white dwarfs (Scaringi et al. 2022). At the level of mmag-precision ground-based photometry, the *RATS* and *OmegaWhite* surveys covered >400 square degrees of Galactic Plane fields at a 5 minute cadence in a single filter (Ramsay & Hakala 2005, Ramsay et al. 2006, Macfarlane et al. 2015). The ZTF High Cadence survey (Kupfer et al. 2021) is hugely successful in finding, among others, ultracompact binaries (e.g. Burdge et al. 2019, Burdge et al. 2020, van Roestel et al. 2022, Burdge et al. 2023). These binaries are also strong sources of gravitational wave emission, but in the lower frequency ranges to be covered by the LISA mission (Ramsay et al. 2018, Kupfer et al. 2023).

To discover and study the population of ultracompact binaries as well as short-period single and close binary pulsators, the BlackGEM array will perform a Fast Synoptic Survey, which will use one telescope continuously. The observing strategy will consist of a 3-4 hr monitor of a single field continuously with 60s exposures while cycling through the filters in a sequence of $(q, u, q, i, q, u, q, i...)$. Hereby, the q-band filter gets a higher cadence than u and i, allowing for shorter duration signals to be resolved (e.g. ingress/egress features of short-period eclipsing systems). Two fields will be observed per night, and each will be repeated the next night for an identical set of observations. In addition, each observed field will be targeted once per night in the q-band with an additional 60s exposure for 14 nights before and after the 2-day high-cadence observations.

7. Science operations and summary

The BlackGEM array was installed at the ESO La Silla Observatory over the period August 2019 - February 2020. All installation and commissioning activities had to be suspended due to the COVID-19 pandemic in March 2020 and could only be resumed in March 2022: a full two-year hiatus due to suspended travel between Europe and South America, closure of ESO sites, and strict travel restrictions on either the European or Chilean sides. Scientific operations started on April 1, 2023 and will run for a five-year period. This first overview paper will be followed by a survey plan paper, a data reduction and data-basing paper, and the commissioning results together with the first-year results on general performance.

The BlackGEM array consists of three 65cm wide-field unit telescopes installed at the ESO La Silla Observatory in Chile. Together they provide an 8.2 square degree field-of-view. Standard survey operations consist of 60s exposures, in one of six filters (u, g, q, r, i, z) that cover the optical wavelength range. The science focus is on time-domain astronomy, in particular counterparts to gravitational wave mergers, in combination with transients in Local Universe (binary) stellar populations and ultracompact binaries in our Milky Way Galaxy. BlackGEM will offer a high-cadence (<1 day), multi-colour view of transients and variables in the Local Universe.

References

Abbott, B. P., Abbott, R., Abbott, T. D., et al. 2016, Phys. Rev. Lett., 116, 061102
Abbott, B. P., Abbott, R., Abbott, T. D., et al. 2020, Living Reviews in Relativity, 23, 3
Abbott, B. P., Abbott, R., Abbott, T. D., et al. 2017a, Phys. Rev. Lett., 119, 161101
Abbott, B. P., Abbott, R., Abbott, T. D., et al. 2017b, ApJ, 848, L12
Abbott, R., Abbott, T. D., Acernese, F., et al. 2023, Physical Review X, 13, 041039
Aerts, C. 2021, Reviews of Modern Physics, 93, 015001
Andreoni, I., Kool, E. C., Sagués Carracedo, A., et al. 2020, ApJ, 904, 155
Arcavi, I., Hosseinzadeh, G., Howell, D. A., et al. 2017, Nature, 551, 64
Bellm, E. C., Kulkarni, S. R., Graham, M. J., et al. 2019, PASP, 131, 018002
Blagorodnova, N., Klencki, J., Pejcha, O., et al. 2021, A&A, 653, A134
Blagorodnova, N., Kotak, R., Polshaw, J., et al. 2017, ApJ, 834, 107
Bloemen, S., Groot, P., Woudt, P., et al. 2016, in Society of Photo-Optical Instrumentation Engineers (SPIE) Conference Series, Vol. 9906, Ground-based and Airborne Telescopes VI, ed. H. J. Hall, R. Gilmozzi, & H. K. Marshall, 990664
Burdge, K. B., Coughlin, M. W., Fuller, J., et al. 2020, ApJ, 905, L7
Burdge, K. B., Coughlin, M. W., Fuller, J., et al. 2019, Nature, 571, 528
Burdge, K. B., El-Badry, K., Rappaport, S., et al. 2023, ApJ, 953, L1
Chambers, K. C., Magnier, E. A., Metcalfe, N., et al. 2016, arXiv e-prints, arXiv:1612.05560
Chase, E. A., O'Connor, B., Fryer, C. L., et al. 2022, ApJ, 927, 163
Córsico, A. H., Althaus, L. G., Miller Bertolami, M. M., & Kepler, S. O. 2019, A&A Rev., 27, 7
de Wet, S., Groot, P. J., Bloemen, S., et al. 2021, A&A, 649, A72
de Wet, S., Izzo, L., Groot, P. J., et al. 2023, A&A, 677, A32
Doi, M., Tanaka, M., Fukugita, M., et al. 2010, AJ, 139, 1628

Drew, J. E., Gonzales-Solares, E., Greimel, R., et al. 2016, VizieR Online Data Catalog, II/341
Drew, J. E., Gonzalez-Solares, E., Greimel, R., et al. 2014, MNRAS, 440, 2036
Drlica-Wagner, A., Ferguson, P. S., Adamów, M., et al. 2022, ApJS, 261, 38
Fairhurst, S. 2011, Classical and Quantum Gravity, 28, 105021
Gaia Collaboration, Vallenari, A., Brown, A. G. A., et al. 2023, A&A, 674, A1
Ghosh, S., Bloemen, S., Nelemans, G., Groot, P. J., & Price, L. R. 2016, A&A, 592, A82
Giammichele, N., Charpinet, S., Fontaine, G., et al. 2018, Nature, 554, 73
Gompertz, B. P., Cutter, R., Steeghs, D., et al. 2020, MNRAS, 497, 726
Grossman, D., Korobkin, O., Rosswog, S., & Piran, T. 2014, MNRAS, 439, 757
Harmer, C. F. W. & Wynne, C. G. 1976, MNRAS, 177, 25P
Hermes, J. J., Gänsicke, B. T., Kawaler, S. D., et al. 2017, ApJS, 232, 23
Horne, K. 1986, PASP, 98, 609
Hosenie, Z., Bloemen, S., Groot, P., et al. 2021, Experimental Astronomy, 51, 319
Kasen, D., Badnell, N. R., & Barnes, J. 2013, ApJ, 774, 25
Kasliwal, M. M., Anand, S., Ahumada, T., et al. 2020, ApJ, 905, 145
Kawaguchi, K., Shibata, M., & Tanaka, M. 2020, ApJ, 889, 171
Kozłowski, S. K., Sybilski, P. W., Konacki, M., et al. 2017, PASP, 129, 105001
Kupfer, T., Korol, V., Littenberg, T. B., et al. 2023, arXiv e-prints, arXiv:2302.12719
Kupfer, T., Prince, T. A., van Roestel, J., et al. 2021, MNRAS, 505, 1254
Lindegren, L., Klioner, S. A., Hernández, J., et al. 2021, A&A, 649, A2
Macfarlane, S. A., Toma, R., Ramsay, G., et al. 2015, MNRAS, 454, 507
McCarthy, D. D. & Petit, G. 2004, IERS Technical Note, 32, 1
Nissanke, S., Kasliwal, M., & Georgieva, A. 2013, ApJ, 767, 124
Onken, C. A., Wolf, C., Bessell, M. S., et al. 2024, arXiv e-prints, arXiv:2402.02015
Petrov, P., Singer, L. P., Coughlin, M. W., et al. 2022, ApJ, 924, 54
Qin, Y.-J., Zhang, K., Bloom, J., et al. 2023, arXiv e-prints, arXiv:2309.10022
Ramsay, G., Green, M. J., Marsh, T. R., et al. 2018, A&A, 620, A141
Ramsay, G. & Hakala, P. 2005, MNRAS, 360, 314
Ramsay, G., Napiwotzki, R., Hakala, P., & Lehto, H. 2006, MNRAS, 371, 957
Ranaivomanana, P., Johnston, C., Groot, P. J., et al. 2023, A&A, 672, A69
Raskin, G., Bloemen, S., Morren, J., et al. 2013, A&A, 559, A26
Raskin, G., Morren, J., Pessemier, W., et al. 2016, in Society of Photo-Optical Instrumentation Engineers (SPIE) Conference Series, Vol. 9908, Ground-based and Airborne Instrumentation for Astronomy VI, ed. C. J. Evans, L. Simard, & H. Takami, 99084L
Rosswog, S., Korobkin, O., Arcones, A., Thielemann, F. K., & Piran, T. 2014, MNRAS, 439, 744
Scaringi, S., de Martino, D., Buckley, D. A. H., et al. 2022, Nature Astronomy, 6, 98
Scaringi, S., Maccarone, T. J., Kording, E., et al. 2015, Science Advances, 1, e1500686
Setzer, C. N., Peiris, H. V., Korobkin, O., & Rosswog, S. 2023, MNRAS, 520, 2829
Smartt, S. J. 2015, PASA, 32, e016
Smith, N., Li, W., Silverman, J. M., Ganeshalingam, M., & Filippenko, A. V. 2011, MNRAS, 415, 773
Steeghs, D., Galloway, D. K., Ackley, K., et al. 2022, MNRAS, 511, 2405
ter Horst, R., Kragt, J., Lesman, D., & Navarro, R. 2016, in Society of Photo-Optical Instrumentation Engineers (SPIE) Conference Series, Vol. 9912, Advances in Optical and Mechanical Technologies for Telescopes and Instrumentation II, ed. R. Navarro & J. H. Burge, 99121J
Toma, R., Ramsay, G., Macfarlane, S., et al. 2016, MNRAS, 463, 1099
Tonry, J. L., Denneau, L., Heinze, A. N., et al. 2018, PASP, 130, 064505
Uzundag, M., Vučković, M., Németh, P., et al. 2021, A&A, 651, A121
van Roestel, J., Groot, P. J., Kupfer, T., et al. 2019a, MNRAS, 484, 4507
van Roestel, J., Groot, P. J., Kupfer, T., et al. 2019b, MNRAS, 484, 4507
van Roestel, J., Kupfer, T., Green, M. J., et al. 2022, MNRAS, 512, 5440
Zackay, B., Ofek, E. O., & Gal-Yam, A. 2016, ApJ, 830, 27

1 Department of Astrophysics/IMAPP, Radboud University, P.O. Box 9010, 6500 GL, Nijmegen, The Netherlands
e-mail: s.bloemen,p.groot@astro.ru.nl
2 Department of Astronomy, University of Cape Town, Private Bag X3, Rondebosch, 7701, South Africa
3 South African Astronomical Observatory, P.O. Box 9, Observatory, 7935, South Africa
4 The Inter-University Institute for Data Intensive Astronomy, University of Cape Town, Private Bag X3, Rondebosch, 7701, South Africa
5 Anton Pannekoek Institute for Astronomy, University of Amsterdam, P.O. Box 94249, 1090 GE Amsterdam, The Netherlands
6 Instituut voor Sterrenkunde, KU Leuven, Celestijnenlaan 200D, 3001 Leuven, Belgium
7 SRON, Netherlands Institute for Space Research, Niels Bohrweg 4, 2333 CA, Leiden, The Netherlands
8 Leiden Observatory, Leiden University, P.O. Box 9513, NL-2300 RA Leiden, The Netherlands
9 NOVA, Netherlands Research School for Astronomy, P.O. Box 9513, NL-2300 RA Leiden, The Netherlands
10 Max Planck Institute for Astronomy, Königstuhl 17, 69117, Heidelberg, Germany
11 TechnoCenter, Faculty of Science, Radboud University, P.O. Box 9010, 6500 GL, Nijmegen, The Netherlands
12 Center for Mathematics and Computer Science, CWI, P.O. Box 94079, 1090 GB Amsterdam,The Netherlands
13 School of Physics and Astronomy, Tel Aviv University, Tel Aviv 69978, Israel
14 Departament de Física Quántica i Astrofísica (FQA), Universitat de Barcelona (UB), Barcelona, Spain
15 Institut de Ciéncies del Cosmos (ICCUB), Universitat de Barcelona (UB), Barcelona, Spain
16 Institut d'Estudis Espacials de Catalunya (IEEC), Barcelona, Spain
17 Department of Physics and Astronomy, The University of Manchester, Oxford Road, Manchester, M13 9PL, United Kingdom
18 Institut für Physik und Astronomie, Universität Potsdam, Haus 28, Karl-Liebknecht-Str. 24/25, D-14476 Potsdam-Golm, Germany
19 Kapteyn Astronomical Institute, University of Groningen, PO Box 800, 9700 AV Groningen, The Netherlands
20 Department of Physics & Astronomy, Texas Tech University, Box 41051, Lubbock, TX, USA, 79409-1051
21 Department of Particle Physics and Astrophysics, Weizmann Institute of Science, 234 Herzl St., Rehovot, 76100, Israel
22 Racah Institute of Physics. The Hebrew University of Jerusalem. Jerusalem 91904, Israel
23 Max-Planck-Institut für Astrophysik, Karl-Schwarzschild-Straße 1, 85741 Garching bei München, Germany
24 Hamburger Sternwarte, University of Hamburg, Gojenbergsweg 112, D-21029 Hamburg, Germany
25 DTU Space, National Space Institute, Technical University of Denmark, Elektrovej 327, 2800 Kgs. Lyngby, Denmark
26 Department of Physics, Gibbet Hill Road, University of Warwick, Coventry CV4 7AL, United Kingdom
27 Centre for Extragalactic Astronomy, Ogden Centre for Fundament Physics - West, Department of Physics, Durham University, South Road, Durham DH1 3LE
28 European Southern Observatory, Karl-Schwardschildstraße 2, Garching-bei-Munchen, Germany
29 Armagh Observatory & Planetarium, College Hill, Armagh, BT61 9DG, Northern Ireland, UK
30 Gemini Observatory, NSF's NOIRLab, Av. J. Cisternas 1500 N, 1720236 La Serena, Chile
31 Thüringer Landessternwarte Tautenburg, Sternwarte 5, D-07778 Tautenburg, Germany
32 Department of Physics and Astronomy, University of California, Davis, 1 Shields Avenue, Davis, CA 95616-5270, USA

Appendix A: Filter Measurements

Table A.1. Relative transmission of the BlackGEM filter curves, in 5nm bins. A full resolution version is provided electronically.

λ (nm)	u_{BG}	g_{BG}	q_{BG}	r_{BG}	i_{BG}	z_{BG}
292.25	0.000	0.000	0.000	0.000	0.000	0.000
297.25	0.000	0.000	0.000	0.000	0.000	0.000
302.25	0.000	0.000	0.000	0.000	0.000	0.000
307.25	0.000	0.000	0.000	0.000	0.000	0.000
312.25	0.000	0.001	0.000	0.000	0.000	0.000
317.25	0.000	0.011	0.001	0.002	0.000	0.000
322.25	0.000	0.000	0.000	0.000	0.000	0.000
327.25	0.000	0.000	0.000	0.001	0.000	0.001
332.25	0.001	0.000	0.000	0.000	0.000	0.006
337.25	0.002	0.000	0.000	0.000	0.000	0.001
342.25	0.096	0.000	0.000	0.000	0.000	0.000
347.25	22.166	0.000	0.000	0.000	0.000	0.000
352.25	92.958	0.000	0.000	0.000	0.000	0.000
357.25	96.683	0.000	0.000	0.000	0.000	0.000
362.25	97.085	0.000	0.000	0.000	0.000	0.000
367.25	97.545	0.000	0.000	0.000	0.000	0.001
372.25	97.296	0.000	0.000	0.000	0.001	0.000
377.25	97.328	0.000	0.000	0.001	0.000	0.000
382.25	97.208	0.000	0.000	0.000	0.000	0.000
387.25	96.446	0.000	0.000	0.000	0.000	0.000
392.25	96.367	0.000	0.000	0.000	0.000	0.000
397.25	96.642	0.000	0.000	0.000	0.000	0.000
402.25	96.305	0.006	0.000	0.000	0.000	0.000
407.25	57.628	0.466	0.000	0.000	0.000	0.000
412.25	0.030	70.832	0.000	0.000	0.000	0.001
417.25	0.000	96.467	0.000	0.000	0.000	0.002
422.25	0.000	96.786	0.000	0.000	0.000	0.000
427.25	0.000	97.458	0.000	0.000	0.000	0.000
432.25	0.000	97.964	0.002	0.000	0.000	0.000
437.25	0.000	98.265	5.539	0.000	0.000	0.000
442.25	0.001	98.545	82.212	0.000	0.000	0.000
447.25	0.000	98.629	97.310	0.000	0.000	0.000
452.25	0.000	98.357	97.653	0.000	0.000	0.000
457.25	0.000	98.402	97.549	0.000	0.000	0.000
462.25	0.000	98.275	97.799	0.000	0.000	0.000
467.25	0.000	97.986	97.747	0.000	0.000	0.000
472.25	0.000	98.032	97.708	0.000	0.000	0.001
477.25	0.000	98.148	97.624	0.000	0.000	0.001
482.25	0.000	97.995	97.772	0.000	0.000	0.000
487.25	0.000	98.326	97.856	0.000	0.000	0.000
492.25	0.000	98.237	97.740	0.000	0.000	0.000
497.25	0.000	98.239	97.831	0.000	0.000	0.000
502.25	0.000	98.556	97.965	0.000	0.000	0.000
507.25	0.000	98.201	97.385	0.000	0.000	0.000
512.25	0.001	98.172	97.685	0.000	0.000	0.000
517.25	0.000	98.363	97.062	0.000	0.000	0.000
522.25	0.000	98.098	97.442	0.000	0.000	0.000
527.25	0.000	97.788	97.577	0.000	0.000	0.000
532.25	0.000	98.153	97.882	0.000	0.000	0.000
537.25	0.000	98.021	97.794	0.000	0.000	0.000
542.25	0.000	97.273	97.573	0.000	0.000	0.000
547.25	0.000	79.142	97.722	0.000	0.000	0.000
552.25	0.000	1.203	97.751	0.000	0.000	0.000
557.25	0.000	0.002	97.261	0.239	0.000	0.000
562.25	0.000	0.001	97.608	63.827	0.000	0.000
567.25	0.000	0.001	97.916	98.437	0.000	0.000
572.25	0.000	0.000	97.612	98.487	0.000	0.000
577.25	0.000	0.000	97.233	98.939	0.000	0.000
582.25	0.001	0.000	97.514	98.933	0.000	0.000
587.25	0.000	0.000	97.649	98.950	0.000	0.000
592.25	0.000	0.000	97.833	98.979	0.000	0.000
597.25	0.001	0.000	97.715	98.960	0.000	0.000
602.25	0.001	0.000	97.891	99.075	0.000	0.000
607.25	0.002	0.000	97.905	99.080	0.000	0.000
612.25	0.001	0.000	97.949	99.067	0.000	0.000
617.25	0.001	0.000	98.255	99.112	0.000	0.000
622.25	0.001	0.000	98.371	99.110	0.000	0.000
627.25	0.001	0.000	98.272	99.097	0.000	0.000
632.25	0.000	0.000	98.081	99.012	0.000	0.000
637.25	0.001	0.000	98.117	99.029	0.000	0.000
642.25	0.000	0.000	98.101	98.988	0.000	0.000
647.25	0.000	0.000	98.182	98.896	0.000	0.000
652.25	0.000	0.000	98.467	98.854	0.000	0.000

Table A.1. , continued

λ (nm)	u_{BG}	g_{BG}	q_{BG}	r_{BG}	i_{BG}	z_{BG}
657.25	0.000	0.000	98.539	98.878	0.001	0.000
662.25	0.000	0.000	98.334	98.986	0.000	0.000
667.25	0.001	0.000	98.127	98.974	0.000	0.000
672.25	0.001	0.000	98.199	98.340	0.000	0.000
677.25	0.001	0.000	98.150	98.793	0.000	0.000
682.25	0.000	0.000	98.123	97.319	0.002	0.000
687.25	0.001	0.000	98.161	57.822	7.231	0.000
692.25	0.001	0.000	98.432	0.174	91.458	0.000
697.25	0.001	0.000	98.174	0.001	98.784	0.000
702.25	0.001	0.000	97.971	0.001	99.037	0.000
707.25	0.001	0.000	97.917	0.000	99.088	0.000
712.25	0.002	0.000	96.086	0.000	99.115	0.000
717.25	0.001	0.000	85.231	0.000	99.034	0.000
722.25	0.000	0.000	8.205	0.000	99.275	0.000
727.25	0.001	0.000	0.024	0.000	99.307	0.000
732.25	0.002	0.000	0.005	0.000	99.285	0.000
737.25	0.001	0.000	0.000	0.000	99.238	0.000
742.25	0.001	0.000	0.000	0.000	99.343	0.001
747.25	0.001	0.000	0.000	0.001	99.344	0.001
752.25	0.001	0.000	0.001	0.000	99.358	0.000
757.25	0.001	0.000	0.005	0.000	99.293	0.000
762.25	0.001	0.000	0.001	0.000	99.382	0.000
767.25	0.001	0.000	0.000	0.000	99.427	0.000
772.25	0.001	0.000	0.000	0.002	99.395	0.000
777.25	0.001	0.000	0.001	0.000	99.322	0.000
782.25	0.001	0.000	0.001	0.000	99.306	0.000
787.25	0.001	0.000	0.000	0.001	99.344	0.000
792.25	0.000	0.000	0.000	0.000	99.258	0.000
797.25	0.000	0.000	0.000	0.000	99.325	0.000
802.25	0.000	0.000	0.000	0.000	98.956	0.000
807.25	0.000	0.000	0.000	0.001	99.023	0.000
812.25	0.000	0.000	0.000	0.000	99.024	0.000
817.25	0.000	0.000	0.000	0.000	98.978	0.000
822.25	0.002	0.000	0.000	0.000	98.937	0.000
827.25	0.002	0.000	0.000	0.000	98.821	0.001
832.25	0.002	0.000	0.000	0.000	98.248	0.020
837.25	0.002	0.000	0.000	0.000	92.816	4.992
842.25	0.002	0.000	0.000	0.000	10.020	82.218
847.25	0.001	0.000	0.000	0.000	0.031	97.964
852.25	0.001	0.000	0.000	0.000	0.002	99.124
857.25	0.001	0.000	0.000	0.000	0.001	98.764
862.25	0.000	0.000	0.000	0.000	0.001	99.076
867.25	0.000	0.000	0.000	0.000	0.001	98.628
872.25	0.000	0.000	0.000	0.001	0.001	98.586
877.25	0.000	0.000	0.000	0.001	0.001	98.683
882.25	0.000	0.000	0.000	0.002	0.000	99.010
887.25	0.000	0.000	0.000	0.001	0.000	98.841
892.25	0.000	0.000	0.000	0.000	0.000	98.842
897.25	0.000	0.000	0.000	0.000	0.001	98.987
902.25	0.000	0.000	0.000	0.001	0.000	98.857
907.25	0.001	0.000	0.000	0.000	0.000	99.079
912.25	0.000	0.000	0.000	0.000	0.000	99.054
917.25	0.000	0.000	0.000	0.001	0.000	99.204
922.25	0.000	0.000	0.000	0.001	0.000	99.068
927.25	0.000	0.000	0.000	0.000	0.000	99.056
932.25	0.000	0.000	0.000	0.000	0.000	99.095
937.25	0.000	0.000	0.000	0.000	0.000	99.234
942.25	0.000	0.000	0.000	0.000	0.000	99.058
947.25	0.000	0.000	0.000	0.000	0.000	99.110
952.25	0.001	0.000	0.000	0.000	0.000	99.154
957.25	0.002	0.000	0.000	0.000	0.000	99.155
962.25	0.005	0.000	0.000	0.000	0.000	99.077
967.25	0.004	0.000	0.000	0.000	0.000	99.118
972.25	0.002	0.000	0.000	0.000	0.000	98.900
977.25	0.002	0.000	0.000	0.000	0.000	98.465
982.25	0.001	0.000	0.000	0.000	0.000	97.255
987.25	0.002	0.000	0.000	0.000	0.000	88.720
992.25	0.004	0.000	0.000	0.000	0.000	14.360
997.25	0.007	0.000	0.000	0.000	0.000	0.158
1002.25	0.005	0.000	0.000	0.001	0.000	0.014
1007.25	0.002	0.000	0.000	0.001	0.000	0.005
1012.25	0.001	0.000	0.000	0.003	0.000	0.002
1017.25	0.001	0.000	0.000	0.002	0.000	0.001
1022.25	0.001	0.000	0.000	0.000	0.000	0.001

Table A.2. Total system transmission from the top of the atmosphere for the BlackGEM telescopes, in 5nm bins. A full resolution version is provided electronically.

λ (nm)	u_{BG}	g_{BG}	q_{BG}	r_{BG}	i_{BG}	z_{BG}
292.25	0.000	0.000	0.000	0.000	0.000	0.000
297.25	0.000	0.000	0.000	0.000	0.000	0.000
302.25	0.000	0.000	0.000	0.000	0.000	0.000
307.25	0.000	0.000	0.000	0.000	0.000	0.000
312.25	0.000	0.000	0.000	0.000	0.000	0.000
317.25	0.000	0.000	0.000	0.000	0.000	0.000
322.25	0.000	0.000	0.000	0.000	0.000	0.000
327.25	0.000	0.000	0.000	0.000	0.000	0.000
332.25	0.000	0.000	0.000	0.000	0.000	0.000
337.25	0.000	0.000	0.000	0.000	0.000	0.000
342.25	0.000	0.000	0.000	0.000	0.000	0.000
347.25	0.038	0.000	0.000	0.000	0.000	0.000
352.25	0.174	0.000	0.000	0.000	0.000	0.000
357.25	0.204	0.000	0.000	0.000	0.000	0.000
362.25	0.228	0.000	0.000	0.000	0.000	0.000
367.25	0.251	0.000	0.000	0.000	0.000	0.000
372.25	0.270	0.000	0.000	0.000	0.000	0.000
377.25	0.289	0.000	0.000	0.000	0.000	0.000
382.25	0.308	0.000	0.000	0.000	0.000	0.000
387.25	0.324	0.000	0.000	0.000	0.000	0.000
392.25	0.344	0.000	0.000	0.000	0.000	0.000
397.25	0.364	0.000	0.000	0.000	0.000	0.000
402.25	0.382	0.000	0.000	0.000	0.000	0.000
407.25	0.238	0.002	0.000	0.000	0.000	0.000
412.25	0.000	0.310	0.000	0.000	0.000	0.000
417.25	0.000	0.439	0.000	0.000	0.000	0.000
422.25	0.000	0.458	0.000	0.000	0.000	0.000
427.25	0.000	0.479	0.000	0.000	0.000	0.000
432.25	0.000	0.498	0.000	0.000	0.000	0.000
437.25	0.000	0.515	0.029	0.000	0.000	0.000
442.25	0.000	0.531	0.443	0.000	0.000	0.000
447.25	0.000	0.545	0.537	0.000	0.000	0.000
452.25	0.000	0.556	0.552	0.000	0.000	0.000
457.25	0.000	0.568	0.563	0.000	0.000	0.000
462.25	0.000	0.578	0.575	0.000	0.000	0.000
467.25	0.000	0.587	0.585	0.000	0.000	0.000
472.25	0.000	0.595	0.594	0.000	0.000	0.000
477.25	0.000	0.603	0.600	0.000	0.000	0.000
482.25	0.000	0.612	0.610	0.000	0.000	0.000
487.25	0.000	0.622	0.619	0.000	0.000	0.000
492.25	0.000	0.629	0.626	0.000	0.000	0.000
497.25	0.000	0.636	0.633	0.000	0.000	0.000
502.25	0.000	0.642	0.638	0.000	0.000	0.000
507.25	0.000	0.645	0.640	0.000	0.000	0.000
512.25	0.000	0.652	0.648	0.000	0.000	0.000
517.25	0.000	0.658	0.649	0.000	0.000	0.000
522.25	0.000	0.660	0.656	0.000	0.000	0.000
527.25	0.000	0.660	0.659	0.000	0.000	0.000
532.25	0.000	0.665	0.664	0.000	0.000	0.000
537.25	0.000	0.669	0.668	0.000	0.000	0.000
542.25	0.000	0.667	0.669	0.000	0.000	0.000
547.25	0.000	0.545	0.673	0.000	0.000	0.000
552.25	0.000	0.008	0.676	0.000	0.000	0.000
557.25	0.000	0.000	0.675	0.002	0.000	0.000
562.25	0.000	0.000	0.677	0.443	0.000	0.000
567.25	0.000	0.000	0.679	0.683	0.000	0.000
572.25	0.000	0.000	0.676	0.682	0.000	0.000
577.25	0.000	0.000	0.675	0.686	0.000	0.000
582.25	0.000	0.000	0.684	0.694	0.000	0.000
587.25	0.000	0.000	0.687	0.696	0.000	0.000
592.25	0.000	0.000	0.686	0.694	0.000	0.000
597.25	0.000	0.000	0.689	0.698	0.000	0.000
602.25	0.000	0.000	0.694	0.702	0.000	0.000
607.25	0.000	0.000	0.697	0.705	0.000	0.000
612.25	0.000	0.000	0.701	0.709	0.000	0.000
617.25	0.000	0.000	0.706	0.712	0.000	0.000
622.25	0.000	0.000	0.708	0.713	0.000	0.000
627.25	0.000	0.000	0.701	0.707	0.000	0.000
632.25	0.000	0.000	0.706	0.713	0.000	0.000
637.25	0.000	0.000	0.714	0.720	0.000	0.000
642.25	0.000	0.000	0.717	0.724	0.000	0.000
647.25	0.000	0.000	0.715	0.720	0.000	0.000
652.25	0.000	0.000	0.720	0.723	0.000	0.000

Table A.2. , continued

λ (nm)	u_{BG}	g_{BG}	q_{BG}	r_{BG}	i_{BG}	z_{BG}
657.25	0.000	0.000	0.722	0.725	0.000	0.000
662.25	0.000	0.000	0.724	0.729	0.000	0.000
667.25	0.000	0.000	0.724	0.730	0.000	0.000
672.25	0.000	0.000	0.724	0.725	0.000	0.000
677.25	0.000	0.000	0.724	0.729	0.000	0.000
682.25	0.000	0.000	0.723	0.717	0.000	0.000
687.25	0.000	0.000	0.646	0.390	0.046	0.000
692.25	0.000	0.000	0.690	0.001	0.642	0.000
697.25	0.000	0.000	0.710	0.000	0.715	0.000
702.25	0.000	0.000	0.707	0.000	0.715	0.000
707.25	0.000	0.000	0.709	0.000	0.718	0.000
712.25	0.000	0.000	0.695	0.000	0.717	0.000
717.25	0.000	0.000	0.581	0.000	0.672	0.000
722.25	0.000	0.000	0.053	0.000	0.670	0.000
727.25	0.000	0.000	0.000	0.000	0.668	0.000
732.25	0.000	0.000	0.000	0.000	0.685	0.000
737.25	0.000	0.000	0.000	0.000	0.694	0.000
742.25	0.000	0.000	0.000	0.000	0.696	0.000
747.25	0.000	0.000	0.000	0.000	0.692	0.000
752.25	0.000	0.000	0.000	0.000	0.688	0.000
757.25	0.000	0.000	0.000	0.000	0.651	0.000
762.25	0.000	0.000	0.000	0.000	0.346	0.000
767.25	0.000	0.000	0.000	0.000	0.600	0.000
772.25	0.000	0.000	0.000	0.000	0.666	0.000
777.25	0.000	0.000	0.000	0.000	0.661	0.000
782.25	0.000	0.000	0.000	0.000	0.655	0.000
787.25	0.000	0.000	0.000	0.000	0.646	0.000
792.25	0.000	0.000	0.000	0.000	0.638	0.000
797.25	0.000	0.000	0.000	0.000	0.630	0.000
802.25	0.000	0.000	0.000	0.000	0.617	0.000
807.25	0.000	0.000	0.000	0.000	0.611	0.000
812.25	0.000	0.000	0.000	0.000	0.587	0.000
817.25	0.000	0.000	0.000	0.000	0.543	0.000
822.25	0.000	0.000	0.000	0.000	0.546	0.000
827.25	0.000	0.000	0.000	0.000	0.549	0.000
832.25	0.000	0.000	0.000	0.000	0.545	0.000
837.25	0.000	0.000	0.000	0.000	0.519	0.028
842.25	0.000	0.000	0.000	0.000	0.056	0.455
847.25	0.000	0.000	0.000	0.000	0.000	0.534
852.25	0.000	0.000	0.000	0.000	0.000	0.529
857.25	0.000	0.000	0.000	0.000	0.000	0.517
862.25	0.000	0.000	0.000	0.000	0.000	0.507
867.25	0.000	0.000	0.000	0.000	0.000	0.493
872.25	0.000	0.000	0.000	0.000	0.000	0.481
877.25	0.000	0.000	0.000	0.000	0.000	0.468
882.25	0.000	0.000	0.000	0.000	0.000	0.456
887.25	0.000	0.000	0.000	0.000	0.000	0.441
892.25	0.000	0.000	0.000	0.000	0.000	0.424
897.25	0.000	0.000	0.000	0.000	0.000	0.374
902.25	0.000	0.000	0.000	0.000	0.000	0.365
907.25	0.000	0.000	0.000	0.000	0.000	0.354
912.25	0.000	0.000	0.000	0.000	0.000	0.336
917.25	0.000	0.000	0.000	0.000	0.000	0.324
922.25	0.000	0.000	0.000	0.000	0.000	0.330
927.25	0.000	0.000	0.000	0.000	0.000	0.302
932.25	0.000	0.000	0.000	0.000	0.000	0.190
937.25	0.000	0.000	0.000	0.000	0.000	0.193
942.25	0.000	0.000	0.000	0.000	0.000	0.198
947.25	0.000	0.000	0.000	0.000	0.000	0.188
952.25	0.000	0.000	0.000	0.000	0.000	0.185
957.25	0.000	0.000	0.000	0.000	0.000	0.183
962.25	0.000	0.000	0.000	0.000	0.000	0.185
967.25	0.000	0.000	0.000	0.000	0.000	0.195
972.25	0.000	0.000	0.000	0.000	0.000	0.186
977.25	0.000	0.000	0.000	0.000	0.000	0.171
982.25	0.000	0.000	0.000	0.000	0.000	0.164
987.25	0.000	0.000	0.000	0.000	0.000	0.142
992.25	0.000	0.000	0.000	0.000	0.000	0.022
997.25	0.000	0.000	0.000	0.000	0.000	0.000
1002.25	0.000	0.000	0.000	0.000	0.000	0.000
1007.25	0.000	0.000	0.000	0.000	0.000	0.000
1012.25	0.000	0.000	0.000	0.000	0.000	0.000
1017.25	0.000	0.000	0.000	0.000	0.000	0.000
1022.25	0.000	0.000	0.000	0.000	0.000	0.000